Phased chromosome-scale genome assembly of an asexual, allopolyploid root-knot nematode reveals complex subgenomic structure

Analysis of the allopolyploid genome of *Meloidogyne javanica*

Michael R Winter[1*], Adam P Taranto[3], Henok Zemene Yimer[2], Alison Coomer Blundell[3], Shahid Siddique[2], Valerie M Williamson[3], and David H Lunt[1]

[1]School of Natural Sciences, University of Hull, Hull, UK

[2]Department of Entomology and Nematology, University of California Davis, Davis CA, USA

[3]Department of Plant Pathology, University of California Davis, Davis CA, USA

*Corresponding author

E-mail: mrmrwinter@gmail.com (MRW)

Abstract

We present the chromosome-scale genome of the allopolyploid root-knot nematode *Meloidogyne javanica*. We show that the *M. javanica* genome is predominantly allotetraploid, comprising two subgenomes, A and B, that most likely originated from hybridisation of two ancestral parental species. The assembly is annotated using full-length non-chimeric transcripts, comparison to reference databases, and *ab initio* prediction techniques, and the subgenomes are phased using ancestral k-mer spectral analysis. Subgenome B appears to show greater fission of chromosomal contigs, and while there is substantial synteny between subgenomes, we also identify regions lacking synteny that may have diverged in the ancestral genomes prior to or following hybridisation. Indels are common both between alleles within a subgenome, and between the A and B subgenomes, suggesting the *M. javanica* genome exists in a dynamic hypo-tetraploidy where copy number can vary along the chromosome. This annotated and phased genome assembly forms a significant resource for understanding the origins and genetics of these globally important plant pathogens.

Author Summary

Root-knot nematodes represent one of the most significant crop parasites globally. Despite their agricultural importance, only rudimentary genomic resources have been published to date, leaving a gap in the understanding of genetic mechanisms driving genome evolution and crop virulence. Here, we have used modern genomic and bioinformatic approaches to create a chromosome-scale reference genome to investigate the origins and genomic constitution of the root-knot nematode species *Meloidogyne javanica*. This species reproduces by ameiotic parthenogenesis and has an allopolyploid

genome and is among the most damaging plant parasitic nematodes with a large and evolving plant host range.

Utilising modern long-range DNA sequencing and bioinformatics approaches, we successfully phased the genome into its constituent subgenomes, a first for this agriculturally important clade. While we find the genomic landscape is mostly syntenic between subgenomes, we identified regions of minimal similarity, and highlight structural divergence between subgenomes. We demonstrate that this species was originally tetraploid, but insertions and deletions have been the major force in generating diversity, resulting in a hypo-tetraploid genome with local variations in ploidy.

Introduction

The assembly of allopolyploid genomes

Allopolyploidy is a genomic state characterised by more than two chromosomal complements, with one or more of these complements resulting from a hybridisation event leading to the presence of distinct (homoeologous) subgenomes within a single cell [1]. Allopolyploids may account for 11% of plant species including many model species and important crops [2]. Although not as frequent as in plants, genomic investigations are indicating that ancestral genome duplication, hybridisation, and complex genome arrangements are more widespread than previously recognized in animals [3,4]. Assembly and analysis of allopolyploid genomes, however, is challenging for a number of reasons [5]. The increased number of alleles within an allopolyploid genome can interfere with algorithms used by many assemblers leading to the accumulation of switch errors; regions of the assembly where the sequence switches between haplotypes or homoeologs. In addition, the high amount of repeat content often found in allopolyploid genomes can result

in fragmentation of the final assembly if sequenced reads fail to span the repeat [6,7]. Another difficulty in accurate assembly of allopolyploid genomes has been 'phasing' ie, the assignment of assembly contigs to the correct subgenome. Switch errors and misassemblies introduced during the assembly process can impair the signals required to successfully phase a scaffold, and potential crossover interactions between homoeologs can further complicate this signal [8,9].

Assembly of allopolyploid genomes has become more feasible due to the advent of long-read sequencing technologies and better assembly algorithms. Most chromosome-scale allopolyploid assemblies in the literature are of agricultural plants [10–13], although a few chromosome-scale allopolyploid assemblies of animal genomes are now also available [14,15].

Root-knot nematodes

Root-knot nematodes (RKN) - genus Meloidogyne - are a group of obligate plant parasites that include species which severely reduce crop yield [16]. Second-stage juveniles (J2s) of RKNs hatch in the soil and are non-feeding, needing to invade a host plant root to complete their life cycle. Upon reaching the vascular cylinder, J2s induce the formation of a feeding site inside the root, characterised by formation of a gall ("root-knot") and highly modified "giant cells" on which the nematode feeds [17]. Three closely related species within the Meloidogyne genus, M. arenaria, M. incognita, and M. javanica, which we refer to here as the Meloidogyne incognita group (MIG), have extremely broad host ranges spanning the majority of flowering plants [18,19]) and together are estimated to cost the agricultural industry tens of billions of US dollars a year [20–22]. Almost 100 RKN species have been described [23,24], which differ in host range, pathogenicity, geographic range, morphology and reproductive mode.

Although RKN nematodes species have diverse modes of reproduction including amphimixis, automixis, and obligate apomixis, cytological examination indicates that M. javanica and most other MIG species reproduce by mitotic parthenogenesis; that is, maturation of oocytes consists of a single mitotic division in which chromosomes remain univalent at metaphase [25,26]. Phylogenomic analysis has revealed that each species possesses two divergent copies of many genes, that the three species likely originated from interspecific hybridisation, and that they share the same ancestors who have provided the A and B subgenomes [19,27,28].

Despite asexual reproduction, field isolates and greenhouse selections of MIG species are diverse and successful, differing in their ability to reproduce on specific crop species and varieties (Hartman and Sasser, 1985; [20,29–31]. A widely investigated example is acquisition of ability to reproduce on tomato with the resistance gene Mi-1, which confers effective resistance to MIG species and is widely deployed for nematode management in tomato [32]. Many independent studies have identified MIG populations that are able to break Mi-mediated resistance; these include both field isolates and greenhouse selections of isofemale lines [33,34]. However, efforts to decipher the genetic mechanisms for these phenotypic variants have not so far been successful due in part to the lack of tractable genetics and limitations in genome assemblies. Current MIG genome assemblies are fragmented and the homoeologous genomes are mostly unphased [19,28,35,36] making it difficult to compare homoeologous sequences, gain a true picture of diversity, or to understand the nature of functional variation.

Here we apply a combination of modern genomic and bioinformatic approaches to generate a highly-contiguous, chromosome-level assembly of M. javanica, phased into two subgenomes, creating the first chromosome-scale genome assembly of an apomictic allopolyploid animal that we are aware of. This assembly should provide a very valuable framework for research into the diversity and functional divergence of plant pathogenic

nematode species. In the wider research landscape, genomes such as those from within the MIG can aid in our understanding of adaptation, ploidy, and evolution of genomes following hybridisation events and loss of meiosis [37].

Results

Sequencing and profiling of read libraries

We used PacBio single-molecule real-time (SMRT) sequencing technology, Hi-C chromatin conformation capture, Nanopore long-read sequencing, and Iso-Seq RNA sequencing to generate a genome assembly of *Meloidogyne javanica* strain VW4. Following quality control and concatenation of two libraries, we obtained 2,255,922 PacBio HiFi reads totalling 35.39 gbp (ACC: XXXXXX; S1 Fig). After quality control and concatenation of Oxford Nanopore PromethION data, we obtained 340,373 reads totalling 17.52 gbp (ACC: XXXXXX) (S2 Fig). Our Hi-C library contained 375,330,537 read pairs, of which 26.20% were of sufficiently high quality for scaffolding with *Proximo* (Phase Genomics, WA) (ACC: XXXXXX). After demultiplexing of our Iso-Seq library, we obtained 2,506,897 full-length non-chimeric sequences which collapsed into 59,637 high quality isoforms (ACC: XXXXXX).

Genome-wide k-mer profiling of concatenated PacBio HiFi read libraries with *smudgeplot* [38] indicated that 48% of the genome was tetraploid, 22% was triploid, and 29% was diploid (Fig 1A). However, this analysis likely underestimates the proportion of tetraploid regions, as crossover events or conversion between subgenomic copies can cause homogenisation. An incomplete or hypo-tetraploid state was also indicated using a k-mer spectra approach by *GenomeScope2*, predicting a haploid genome length of 68 mbp,

146 and a duplication rate of 3.4 [38] (Fig. 1B). This duplication rate is similar to the value seen

147 for CEGMA genes in other assemblies of *M. javanica* (3.68) [28].

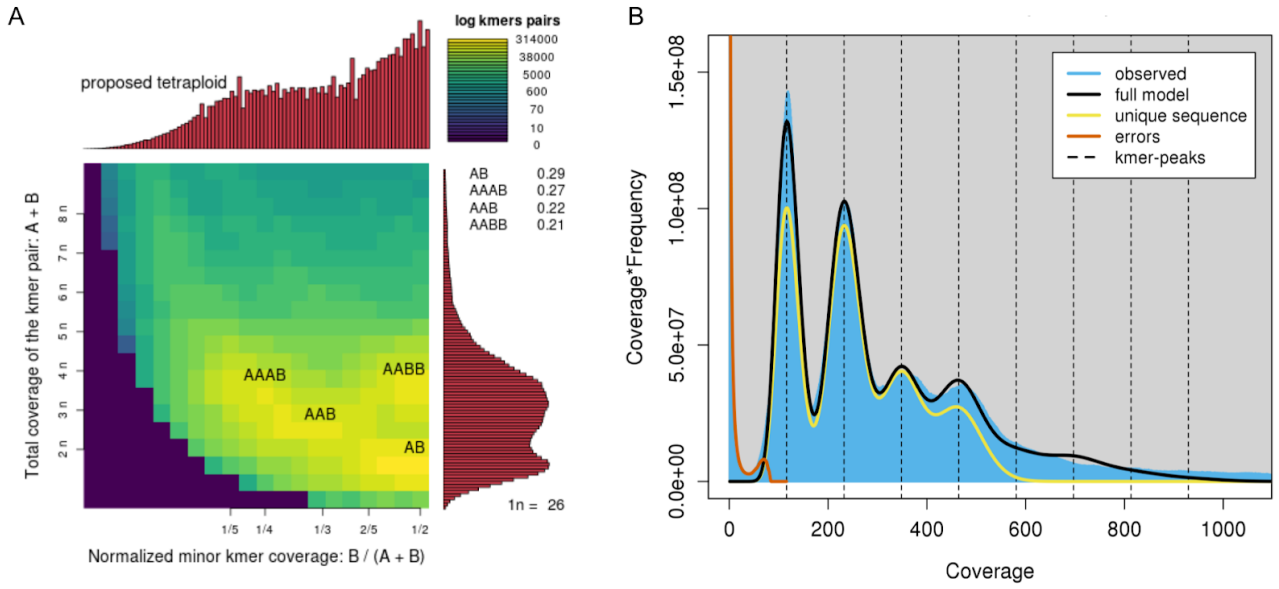

148

149 **Fig 1: Genome profiling plots.**

150 (A) Smudgeplot (left) proposing M. javanica as tetraploid, reporting the predicted

151 percentages of ploidy levels in the genome as follows: tetraploid (48%), triploid (22%), or

152 diploid (29%). (B) GenomeScope2 plot (right) showing four distinct peaks in both the

153 predicted model of tetraploidy (black line) and in the observed k-mer spectra (blue fill). The

154 amount of unique sequence falls to zero shortly after the fourth peak, indicating that k-mers

155 at higher ploidies than four were mostly repetitive elements.

156

157 # Assembly and annotation

158 ## Scaffolding and final assembly

159 From our draft assemblies of the PacBio data, we carried forward an iteration

160 assembled using *HiFiasm* [39] based on overall contiguity and comparison to expected

161 diploid genome length. Following purging of duplicates from the PacBio assembly and

162 scaffolding with Oxford Nanopore reads, we obtained 37 contigs with the N50 of 9.5 mbp.

163 Hi-C scaffolding with the *Proximo* pipeline identified 16 chromosome level clusters (Phase

164 Genomics Ltd), but increased the total number of scaffolds from 37 to 66. Following
165 scaffolding with Hi-C, *samba* [40] joined some small scaffolds and fragmented the largest
166 scaffold in the assembly, increasing the number of scaffolds from 66 to 69.

167 The final assembly scaffolds contains 150,545,692 bp with an N50 of 5,793,182 bp,
168 at 30.11% GC content, and overall, 99.96% of reads in our combined PacBio HiFi library
169 map successfully back to the assembly, indicating a high level of completeness (S1 Table).
170 Of the total assembly, 97.87% was contained in the longest 33 scaffolds (S3 Fig), which
171 ranged from 898 kbp to 9,595 kbp in length (Fig 2A; S6 Table). These 33 scaffolds
172 contained 99.85% of all transcribed gene models. Of the remaining 36 scaffolds, 4 were
173 identified by *blobtools* [41] as likely contaminants (Arthropoda, Chordata, and Streptophyta;
174 S4 Fig). One further contig was the *M. javanica* mitochondrial genome (Scaffold 67). The
175 remaining 31 small contigs were all less than 215 kbp, with a mean length of 88.9 kbp, and
176 since they contained few identifiably functional elements (0.19% of gene models), we
177 excluded them from the final analysis.

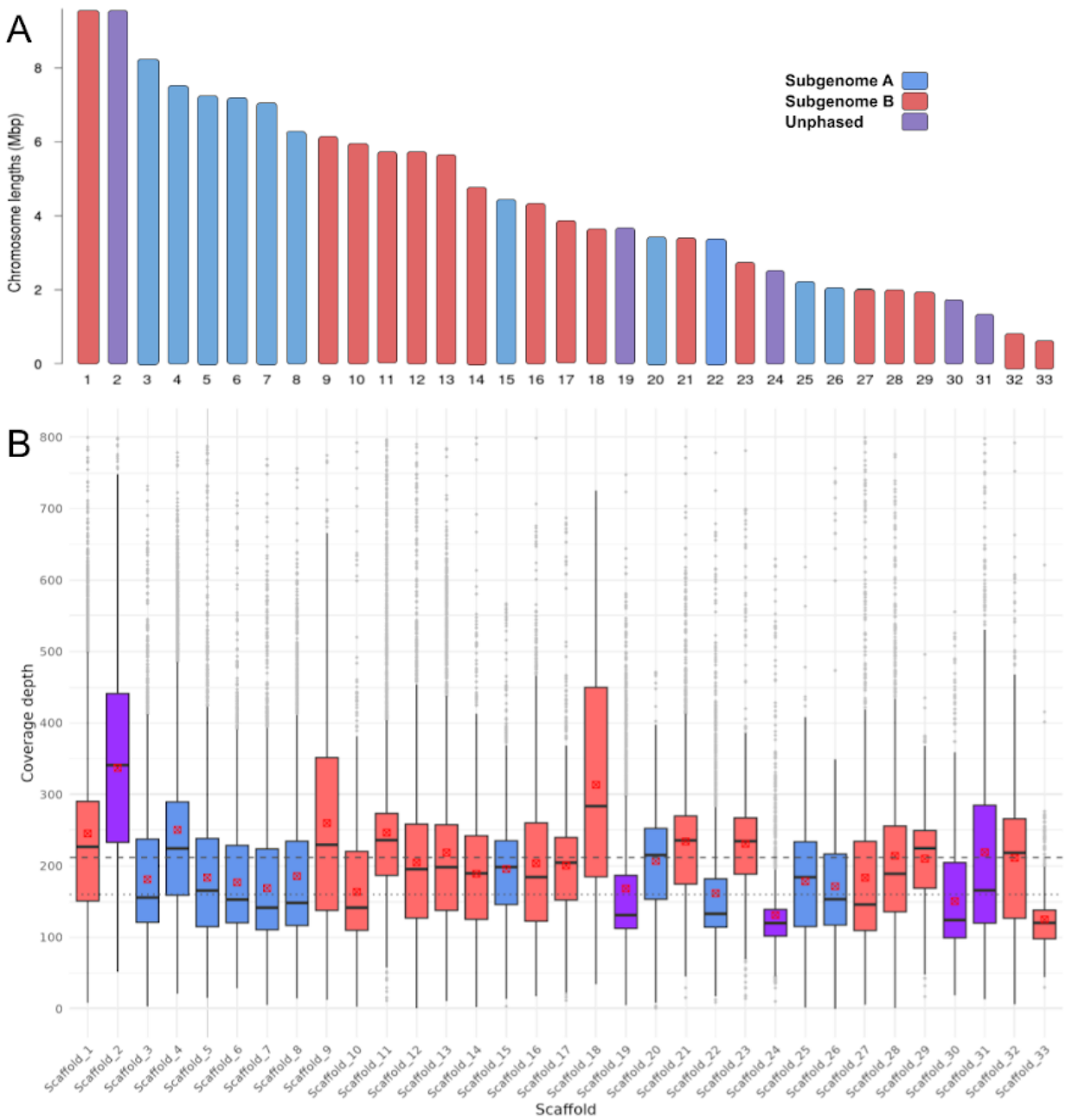

Fig 2. Ideogram and coverage depth of longest 33 scaffolds.

Scaffolds are coloured according to phasing status; blue - subgenome A, red - subgenome B, purple - unphased. A, Ideogram of 33 largest scaffolds. These 33 scaffolds contain 98% the total length of the assembly, with the remaining 36 contigs being shorter than 250 kbp, containing few gene models (0.19%), and consisting of mostly repetitive elements. B, Boxplot displaying the distribution of coverage depth for each scaffold. Red points denote the mean of data in each box. Coverage has been limited to a maximum of 800x to exclude probable repetitive sites with anomalous coverage depth. Dashed line shows the overall

mean for all coverage levels across 33 scaffolds. Dotted line shows the mode of all coverage across 33 scaffolds.

Repeat annotation

In total 30.46% of our assembly was identified as repetitive elements, with 4.94% identified as retroelements, 3.77% as DNA transposons, while 16.88% remain unclassified repeats (S2 Table). A total of 164,394 transcripts, representing 59,632 isoforms, were detected through mapping of our Iso-Seq library. *MAKER3* detected a total of 22,433 genes, containing 227,617 exons, 10,044 5' and 5,253 3' UTRs (S3 Table).

Core Eukaryotic Gene and Single Universal Copy Ortholog Analysis

Analysis of the final assembly with *CEGMA[42]* detected 233 of 248 CEGMA genes (93.95%). This is a higher level of completeness than the most recent *M. javanica* assembly, and comparable with contemporary *Meloidogyne* assemblies [19,36,43,44]

The average number of orthologs for each complete CEGMA gene (a proxy for ploidy) is 1.88 indicating that only ~6% of the diploid genome is unassembled or not present in the biological chromosomes. 173 complete BUSCO genes were detected, representing 67.9% of genes in the BUSCO eukaryote database. Of the BUSCOs identified, 31.4% were duplicated (S5 Fig).

Coverage and ploidy analysis

Mean coverage depth for all scaffolds - excluding mitochondrial - was 206.6x, falling to 206.1x for the longest 33 scaffolds (Fig 2B). For some scaffolds (2, 9 and 18) coverage depth was significantly in excess of this average, indicating collapsed regions; that is, representation of three or four rather than two copies. Collapse is expected to arise in a polyploid assembly when homoeologous sequences are similar enough at a nucleotide level that they are inferred to be multiple homologous alleles of the same region, which are

213 then collapsed to form the reference assembly copy [8]. Other scaffolds (19, 22, 24, 33)
214 were underrepresented suggesting that they may be present as a single copy.

215 We then examined the coverage depth frequency distribution for each scaffold (Sup
216 Fig 7). For phased scaffolds representing two identical homologs, the frequency of
217 coverage for all bases in each scaffold would be expected to have a single peak (240x).
218 However, while predominantly single peaks were seen for under-represented scaffolds
219 thought to be present as a single copy (19, 22, 24, 33), we observed two peaks for the
220 majority of scaffolds (Fig 3A & C; S7 Fig). Two peaks would be expected if homologs are
221 not identical and similarity is disrupted by indels, with the second peak representing the
222 reduced coverage of the hemizygous region (~120x). For scaffold 2, which is over-
223 represented in coverage depth, four clear peaks are present (Fig 3) indicating that more
224 than two copies map to the scaffold. This likely resulted from exclusion of the scaffold's
225 homoeolog from the assembly, leading to an assembly collapse as noted above.
226 Nevertheless, the presence of 4 peaks is consistent with the presence of polymorphisms
227 between homologous copies as well as between homoeologous pairs.

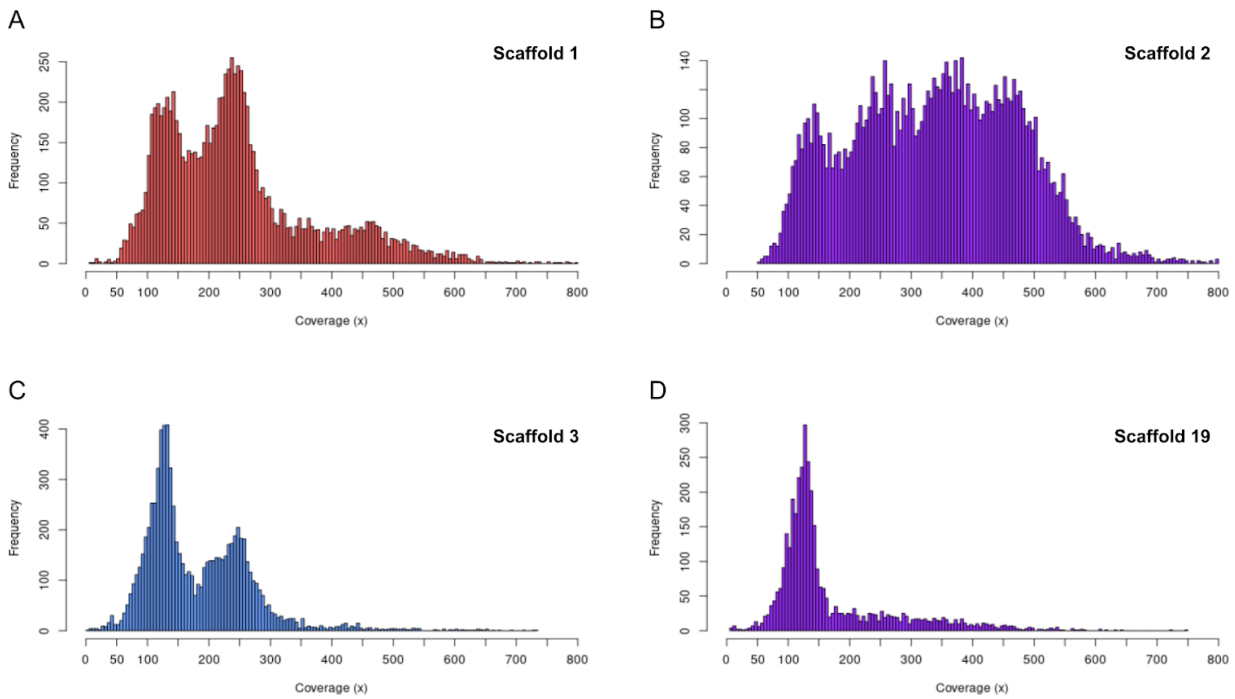

228

229 **Fig 3. Coverage depth frequency distributions of scaffolds 1, 2, 3, and 19.**

230 X-axis represents coverage depth and y-axis represents frequencies of coverage. Colour
231 indicates phase status: red for subgenome B, blue for subgenome A, and purple for
232 unphased scaffolds. (A) Scaffold 1, top left, displays two main peaks of coverage with a
233 small tail suggesting short collapsed regions. (B) Scaffold 2, top right, displays four peaks of
234 coverage, indicating that much of this scaffold is collapsed and four copies are mapping to
235 it. (C) Scaffold 3, bottom left, shows two peaks and very little tail, indicating two copies
236 mapping and little to no assembly collapse. (D) Scaffold 19, bottom right, shows only one
237 peak at ~120x coverage, suggesting that only one copy maps to this scaffold.

238

239 To examine the ploidy distribution in another way, we plotted a sliding window of
240 coverage across each scaffold (S8 Fig). In support of the coverage depth distributions, the
241 most frequent outcome was that scaffolds in the assembly show two layers of stratification
242 in coverage at a constant proportional depth, indicating two copies distinguished by indels
243 between them. This pattern was strongest for scaffolds with two coverage peaks,
244 particularly phased homoeologs (discussed below, Fig. 3 A & B; S7 Fig). Scaffold 2 and
245 scaffold 18, which are over-represented in sequence depth, contain regions of four levels of
246 coverage depth covering much of the length of both (Fig 3B; S8a and 8d Figs). This
247 increased amount of stratification at proportionally higher coverage depths (360x and 480x)
248 reveals assembly collapse, where four copies map to a single site. Together these
249 coverage depth results suggest that the *M. javanica* assembly represents two
250 homoeologous subgenomes (~87% of total length), with only 13% of the assembly
251 unphased or collapsed.

252

253 # Identification of homoeologous pairs and phasing of
254 subgenomes

255 Given the diploid nature of the assembly, which represents each subgenome as a
256 single copy, we expected to find scaffolds from these subgenomes present in
257 homoeologous pairs. Through detection of shared orthologs (Supplementary Methods)
258 twenty pairings were identified between the longest 33 scaffolds of the assembly, each
259 sharing between 20 and 351 CDS orthologs (Fig 4, S4 Table). Alternative methods of
260 identifying homoeologous pairs were corroborative (S5 Table). Some pairs were not
261 mutually exclusive, and exhibited CDS links to scaffolds outside of the primary pair,
262 suggesting translocation and syntenic changes between them. All scaffolds that showed
263 two depths of coverage were assigned as homoeologous pairs as expected if each
264 subgenome was heterozygous. Four scaffolds were excluded from pairings including
265 scaffold 2 which showed high amounts of collapse and scaffolds 19, 24, 30, and 31 which
266 are relatively small and/or present as single copies (S7 Fig and 9; S6 Table).

267 In order to assign contigs to a subgenome, we used a modified version of an
268 ancestral k-mer spectra analysis [45] (Supplementary Methods). This approach is based on
269 the premise that the allopolyploid's subgenomes possess repeats that diverged in the two
270 parental genomes before hybridisation. This results in a distinguishable signature in each
271 subgenome's k-mer spectrum, and allows us to determine the parental species from which
272 a given sequence descends. We successfully phased 85.39% of the genome into A or B
273 subgenomes (Fig 2A; S9 Fig; S6 Table). Scaffold 2, which exhibits extensive assembly
274 collapse, did not phase using these methods. Some smaller scaffolds that did not phase by
275 k-mer based methods were later assigned to a subgenome based on the phase status of
276 their opposing homoeologous scaffold (S6 Table). Of the total length of the final assembly,
277 39.15% was assigned to subgenome A and 46.24% was assigned to subgenome B, leaving
278 only 14.61% unassigned.

Subgenomic synteny analysis

Comparison of annotation of scaffold pairs assigned to subgenomes A and B revealed both long regions of synteny and large structural differences between subgenomes (Fig 4). Scaffold 13 and scaffold 15 are syntenic along almost the entire length of the shorter homoeolog and share high nucleotide similarity throughout. Similarly, scaffold pairs 20 and 23, as well as 17 and 25, share long syntenic blocks of shared CDS and long runs of high nucleotide similarity.

Scaffolds 7 and 10 are syntenic for almost half of their length whilst the remaining sequence lengths share no synteny and have very low nucleotide similarity. Synteny analysis and scaffold comparison suggest that chromosomal fragmentation has occurred. For example, scaffold 8 of subgenome A shows long collinear blocks with scaffolds 16, 28, 29, and 33 of subgenome B. Re-examination of Hi-C and ONT long-read scaffolding as well as manual inspection of read mapping support this fragmentation. Scaffold 1 of subgenome B shares syntenic blocks with scaffolds 5, 6, and 8 of subgenome A, in an order that suggests chromosomal structural differences between the subgenomes. Many phased scaffolds also exhibit small amounts of extra-pair synteny indicating numerous small translocations throughout the genome.

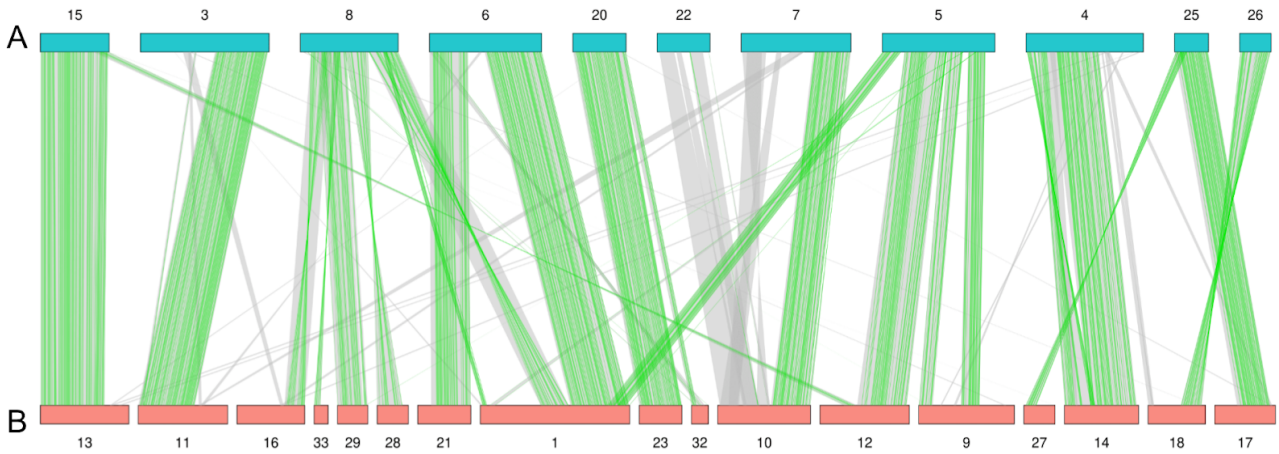

298 **Fig 4. Macrosynteny analysis between subgenomes.**

299 Glyphs along top and bottom represent scaffolds assigned to either subgenome A (blue) or
300 subgenome B (red). Green lines mark locations of synteny between transcribed genes
301 identified from mapping of Iso-Seq sequences. Grey lines mark locations of synteny
302 between genes identified through *MAKER3* gene prediction. Synteny and collinearity were
303 identified using the *MCScan* module of *JCVI* using Iso-Seq informed transcriptional
304 annotation. Scaffolds that could not be assigned to a subgenome are not shown.

305

306

307 Discussion

308 Assembly of the allopolyploid genome of *M. javanica*

309 We have used long-read sequencing and modern bioinformatic approaches to
310 assemble and phase the allopolyploid genome of the plant pathogenic nematode
311 *Meloidogyne javanica*. Our goal was to assemble a contiguous diploid assembly for *M.*
312 *javanica*, representing the A and B subgenomes separately. Our current diploid assembly
313 (150,545,692 bp) is, as expected for a tetraploid, approximately half the 297 ±27Mb
314 measured by flow cytometry [19,28]. This total length is representative of both A and B
315 subgenomes except for collapsed regions where sequence for both subgenomes A and B is
316 considered together. Because some regions of the assembly have been shown by k-mer
317 profiling and coverage analysis to be present in less than four copies (Fig 1; S8 Fig),
318 splitting the subgenomes into their component copies (A1, A2, B1, B2) to create a tetraploid
319 assembly would not be expected to completely double the length.

320 Annotation

321 We annotated our assembly using both *ab initio* feature prediction algorithms and
322 mapping of the full-length transcript sequences (S3 Table). The total number of genes

323 predicted - 22,433 - is within the range expected for a MIG species and is comparable to
324 previous *M. javanica* assemblies [19,28].

325 BUSCO scores for *Meloidogyne* are consistently lower than those of more widely
326 studied organisms, and the number of genes we have detected (S3 Table) in the genome is
327 consistent with what has been found for other *Meloidogyne* species [19,28,46]. The paucity
328 of established protein databases for less frequently investigated genera limits the accuracy
329 of prediction-based annotation methods. Loss of core genes are not unexpected for this
330 group of highly specialised, obligate parasites. With increased availability of sequence
331 resources for plant parasitic nematodes, it should soon be possible to develop a more
332 appropriate set of core genes.

333 Evidence for a chromosome-scale assembly

334 Previous genomic assemblies of *M. javanica* have contig counts numbering in the
335 thousands [19,28]. In our current assembly, more than 99% of reads in our PacBio HiFi
336 libraries map to 33 large scaffolds (Fig 2B). We propose that most of the 33 scaffolds
337 represent full-length or nearly full-length chromosomes. Cytological examination in *M.*
338 *javanica* indicates that the chromosome number ranges from 42-48 due to variation
339 between isolates (Eisenback and Triantaphyllou, 1991; Triantaphyllou 1985, Janssen et al
340 2017). Thus, we would expect 21-24 scaffolds in our assembly. The discrepancy between
341 scaffold number and cytological observations could be due to an imperfect assembly or
342 failure to identify very small chromosomes in the cytological studies. We have employed
343 several independent scaffolding softwares, Hi-C chromatin contact mapping, and the
344 manual examination of long-read mapping to contig termini, and see no evidence to support
345 fusing additional contigs. Additional molecular and cytological studies may be required to
346 resolve these differences.

347 Many chromosome-scale assemblies identify telomeres as defining the range of their
348 scaffolds, yet we did not identify canonical telomeric repeats at scaffold termini.

349 Additionally, we were also not able to identify a homolog of *C. elegans* telomerase (*trt-1;*
350 ACC: NM_001373211.4) in our assembly. This may suggest that non-standard telomere
351 processes might be operating in root-knot nematodes as has been found for fruit flies
352 [49,50].

353

354 Genetic variation in *M. javanica* is dominated by indels

355 We present the assembly as a diploid representation. Read depth analysis of
356 individual scaffolds indicates that homologs are not identical and indels are frequent.
357 Additionally some scaffolds appear to be present as a single copy suggesting that one of
358 the homologs may have been lost. We identified many indels that delete or disrupt one or
359 more copies of coding sequences, indicating that *M. javanica* is no longer genome-wide
360 tetraploid either in copy number or functionality. A higher propensity for indel accumulation
361 has been frequently seen in hybrid parthenogenetic species [51] and partial return to lower
362 ploidy is a characteristic of many polyploids.

363 We find that 87% of our diploid assembly consists of one copy of either subgenome
364 in homoeologous pairs, with two copies mapping to phased scaffolds and four copies
365 mapping to collapsed regions. We successfully phased much of our assembly into
366 subgenomes using k-mer signatures, enabling for the first time initial genome-wide
367 comparison of MIG A and B subgenomes. Some scaffolds, notably scaffold 2 and some of
368 the short scaffolds, could not be assigned to subgenomes. Scaffold 2 displays four levels of
369 stratification in its coverage (S8 Fig) and four peaks in its depth distribution (Fig 3b)
370 indicating that the four copies (A1+A2 and B1+B2) are almost entirely collapsed into a
371 single scaffold. We suggest that the homoeologous chromosomes represented by scaffold
372 2 may be too similar in sequence to assign to a subgenome by k-mer analysis due to a
373 possible homogenization event. For the smaller scaffolds, the failure may have been due to
374 their small size because they did not contain enough relevant k-mers. Some of the small

375 scaffolds were later assigned to a subgenome using transcript alignments. No misassembly
376 or erroneous scaffolding of the unphased sequences was detected through either
377 programmatic or manual methods.

378 The allotetraploid genome of *M. javanica* demonstrates extensive synteny between
379 the A and B subgenomes with most genic regions represented in four copies. We would
380 expect however that there would be differences between the subgenomes, including indels
381 and other structural variation, as this is typically observed between different species and the
382 MIG have a hybrid origin. In accordance with this, we observed very substantial structural
383 variation between subgenomes A and B, including insertions, deletions, and translocations
384 (Fig 4).

385

386 Loss of synteny and fragmentation

387 We observe regions of the *M. javanica* genome where synteny between paired
388 chromosomes is disrupted. One reason for this could be that the parental species (A and B)
389 had genomes in which the non-syntenic regions had diverged by translocation, insertion or
390 deletion. Upon hybridisation to create the allopolyploid MIG these diverged regions form the
391 end of synteny blocks. An alternative explanation is that these changes happened after the
392 hybridisation event in the tumultuous process of genome stabilisation immediately following
393 it [52,53]. Hybridisation, polyploidization, and the loss of meiosis are processes often
394 associated with rapid genomic change [54][51,54,55] and the unique MIG species
395 allopolyploid genomes we are currently studying may represent different balances between
396 these forces. We observe 11 chromosome-scale scaffolds in subgenome A and 17 in
397 subgenome B despite the clear synteny throughout these two genomes. Several scaffolds
398 in subgenome A contain blocks of genes with regions that are syntenic to different
399 subgenome B scaffolds. Similarly, there are cases where syntenic blocks in subgenome B
400 are present on different scaffolds in subgenome A. Together these differences suggest that

401 ancestral chromosomal fission, or fusion events or other types of exchange have occurred.
402 *Meloidogyne* species, like other nematodes, have holocentric chromosomes
403 (Triantaphyllou, 1985). Genomes with dispersed centromere structure are predicted to
404 better tolerate chromosome fragmentation and fusion [56], as are species with ameiotic
405 mechanisms of reproduction. The observed differences in copy number of chromosomes
406 between isolates of *M. javanica* may be additional evidence for tolerance of chromosome
407 fragmentation/fusion. Although it is always necessary to consider the possibility of
408 misassembly or rogue scaffolding, we have substantial evidence through manual inspection
409 and contiguous mapping of ultra-long Oxford Nanopore reads that our assembly is correct.

410 The majority of published assemblies of allopolyploids come from plants, where
411 polyploidy might have shaped the genomes of around 70% of species [57]. Many
412 allopolyploid plant genomes, however, show a higher level of synteny and structural
413 conservation than we observe for *M. javanica* [13,45,58]. Similarly the few available
414 chromosomal allopolyploid animal genome sequences available [14,15] do not show
415 extensive deletions and chromosomal fissions as does our genome. Unlike other
416 allopolyploid species with chromosomal genome sequences, *Meloidogyne javanica*
417 reproduces by obligatory mitotic parthenogenesis (apomixis) and this lack of meiotic
418 chromosome pairing may allow greater structural divergence and tolerance for the decay of
419 synteny. We note that genomes from species not able to reproduce by meiosis are currently
420 rare [51] and suggest that much more substantial genomic work on a range of species with
421 different reproductive modes and ploidy levels will be required to reveal the diverse
422 mechanisms shaping these genomes. It is apparent however that the changes surrounding
423 allopolyploidy have contributed to the gene content, heterozygosity, and copy number
424 throughout the *M. javanica* genome and these processes of locally fixed heterozygosity or
425 rediploidization may contribute extensively to adaptive functional variation [59].

426

427 ## Regional homogenization of subgenomes

428 Some regions of the genome do not phase into A and B homoeologs due to very low
429 divergence between the four gene copies. This could be explained either by the loss of
430 whole chromosomes, compensated by the duplication of the remaining chromosome, or
431 mitotic recombination (gene conversion) between homoeologs [60,61]. It is unclear from
432 this single genome how asexual recombination contributes to shaping the diversity of *M.*
433 *javanica*, however this has been suggested in previous MIG genomic studies [19,28] and
434 may be further elucidated by our ongoing molecular evolution and population genomic
435 studies.

436 The initial tetraploidy of *M. javanica* will buffer against deleterious phenotypic
437 consequences of indels, allowing a substantial accumulation of genetic variation by this
438 mechanism. It has been argued for angiosperms that this rediploidization process can
439 contribute to adaptive species divergence by providing genomic and transcriptomic diversity
440 [59,62]. Other mechanisms of adaptive divergence may also operate at the same time. The
441 increase in gene copy number created by polyploidization gives the potential for functional
442 gene divergence by neo- or sub-functionalization, as well as adaptive phenotypes driven by
443 copy number loss [63–65]. Adaptation by gene copy number variation has already been
444 reported in *M. incognita* [66] and it may be that genomic copy number variation more
445 broadly is a major source of functional genetic variation in the MIG.

446

447 ## A genomic framework for RKN functional and diversity studies

448 In this paper we present a highly contiguous, annotated and phased genome of the
449 allotetraploid plant pathogenic nematode *M. javanica*. This genome assembly will provide
450 many tools for diverse investigations by plant pathologists and nematologists in addition to
451 adding to our understanding of the origins and diversity of *M. javanica*. It will also serve as a

452 reference for investigating genome structure and pathogenicity in other *Meloidogyne*
453 species.

454 The contiguous nature of this genome and the high quality annotation will facilitate
455 RKN functional studies since transcripts can be mapped accurately to the annotated
456 subgenome. This allows consideration of copy number variation, which may be an
457 important component of functional variation in these species.

458 Progress is being made by many groups in understanding the basis of nematode
459 virulence and the key loci involved [67–69]. In such cases even light coverage sequencing
460 of field isolates mapped to a high quality genome could give valuable information to
461 commercial growers about the likely pathogenicity of those strains [70].

462

463

464 Methods

465 Reproducibility

466 Wherever possible, this study attempted to contain all bioinformatic processes in
467 reproducible workflows or scripts, for the purpose of openness and enabling replication.
468 Workflows and code are archived in a Zenodo repository along with final outputs
469 (doi://XXXXXX.XX). The raw reads plus final nuclear and mitochondrial assemblies are
470 available on the International Nucleotide Sequence Databases (INSDC) (ACC: XXXXXX)
471 (ACC: XXXXXX).

472

473 # Biological material

474 *Meloidogyne javanica* strain VW4 was used for this work (Gleason et al, 2008;
475 Szitenberg et al., 2017). Cultures of this strain have been maintained on tomato plants
476 under greenhouse conditions for over 30 years (Yaghoobi et al, 1995). Periodic transfers of
477 single egg masses have been carried out to maintain uniformity. For DNA preparation, eggs
478 were harvested from roots and cleaned by sucrose flotation as previously described
479 (Branch et al, 2004) then flash-frozen in liquid N2. High molecular weight DNA (HMW DNA)
480 isolation was carried out at UC Davis Genome Center (Supplementary Methods). Integrity
481 of the HMW gDNA was verified on a Femto Pulse system (Agilent Technologies, CA) where
482 majority of the DNA was found to be in fragments above 100 Kb.

483 Total RNA was isolated from three *M. javanica* life stages: eggs, freshly hatched
484 juveniles, and females dissected from tomato roots 21 days after infection. This material
485 was flash-frozen and RNA was extracted using an RNeasy Kit (Qiagen, USA) following the
486 manufacturer's instructions. TURBO DNase treatment was carried out to remove genomic
487 DNA from total RNA samples (TURBO DNA-free Kit™, Ambion, USA). RNA concentration
488 and purity were measured using a NanoDrop OneC Microvolume UV-Vis
489 Spectrophotometer (Thermo Scientific, USA). RNA integrity and quality was assessed using
490 bioanalyzer.

491

492 # Sequencing and QC

493 ## High fidelity (HiFi) long-read sequencing

494 PacBio HiFi library preparation and sequencing of HMW DNA was performed by UC
495 Davis DNA Technologies Core on a PacBio Sequel II (Supplementary Methods). Data from
496 the two generated libraries were pooled and only reads longer than 5000 bp and with a
497 quality score over 15 were retained.

498 ## Nanopore sequencing

499 Nanopore sequencing of HMW DNA using Oxford Nanopore Technologies (ONT)
500 systems was carried out by UC Davis DNA Technologies Core. The super-long-read DNA
501 sequencing protocol (Supplementary Methods) yielded 23 gbp of data, which was then
502 filtered to contain only reads longer than 25 kbp.

503 ## Hi-C chromatin conformation capture

504 DNA was prepared using Proximo Hi-C kit (Animal) as recommended by the
505 manufacturer (Phase Genomics, Seattle, WA, USA). Library preparation and sequencing
506 were carried out at the UC Davis DNA Technologies Core and scaffolding with Proximo was
507 performed by Phase Genomics (Supplementary Methods).

508 ## PacBio Iso-Seq

509 Reads from one Sequel II SMRT cell were quality controlled and converted into
510 clustered reads using the *IsoSeq3* pipeline with default parameters [71].

511

512 # Genome profiling

513 Profiling was performed by *Genomescope2* and *smudgeplot [38].* All quality
514 controlled PacBio HiFi libraries were combined and used as input for these programs. Both
515 were run with default parameters, aside from *-ploidy* in *Genomescope2* set to 4, as this was
516 the primary ploidy indicated by *smudgeplot* and suggested by visual analysis of mapped
517 reads.

518

Assembly

Draft assembly

Initial draft assemblies were generated using several different assemblers and appraised with *asmapp [72].* The most appropriate assembly based on length and contiguity was carried forward, after which haplotigs were identified and removed using *purge_dups* [73].

Scaffolding with Oxford Nanopore and Hi-C

We used *SLR* [74] to scaffold the assembly with our trimmed and concatenated ONT reads. The assembly was then scaffolded with Hi-C reads using the *Proximo* pipeline by Phase Genomics Ltd. The resulting contact map was manually curated using *Juicebox* assembly tools [75] to produce the most likely assembly based on contact linkage information and TAD presence or absence. A third phase of scaffolding was performed by *samba,* to break potential misassemblies introduced during manual *Juicebox* scaffolding and scaffold sequences that were broken as debris [40].

Annotation

Repeat annotation

RepeatModeler was applied to the assembly [76], with the resulting library of repeat models used as input for *RepeatMasker* to annotate repeat regions and generate a soft-masked version of the genome [77].

Gene annotation

Iso-Seq reads were mapped to the genome and collapsed using a *snakemake* workflow automating the *IsoSeq3* pipeline [71]. The annotation pipeline *MAKER3* was then

542 employed to perform *ab initio* and predictive annotation of our genome [78,79]. Full
543 methods of annotation iterations and parameters can be found in Supplementary Methods.

544

545 Subgenome phasing

546 Identification of homoeologous scaffold pairs

547 Homoeologous pairs were detected through identification of orthologs shared
548 between scaffolds (Supplementary Methods). Pairs sharing a large number of orthologs
549 and nucleotide similarity were considered homoeologous. This was validated with other
550 methods, including MASH distance [80] and shared possession of duplicated BUSCO
551 genes [81].

552 Phasing of subgenomes

553 Scaffolds were phased into A and B subgenomes using a k-mer-based approach
554 built on the approach taken by [45]. K-mers in the assembly were detected and counted
555 using *jellyfish[82]*, with only k-mers present more than 75 times in the assembly and
556 represented at least twice as often in one subgenome than the other carried forward. These
557 counts were then transformed into binomial distributions. Hierarchical clustering was
558 performed on these sets, creating a dendrogram placing scaffolds into opposing clusters,
559 each cluster representing a subgenome (Supplementary Methods).

560

561 Synteny analysis

562 The *MCScan (Python)* [83] module of *JCVI [84]*was used to perform a synteny
563 analysis between the two subgenomes. Custom scripts then extracted collinearity
564 information and generated synteny plots (Supplementary Methods).

565

566

567 # Acknowledgments

568 We acknowledge the Viper High Performance Computing facility of the University of
569 Hull and its support team, specifically Chris Collins, for their invaluable help in managing
570 and deploying software, as well as the high Performance Computing team at UC Davis for
571 making available their resources for part of our analysis.

572

573

574 # References

575 1. Glover NM, Redestig H, Dessimoz C. Homoeologs: What Are They and How Do We
576 Infer Them? Trends Plant Sci. 2016;21: 609–621. doi:10.1016/j.tplants.2016.02.005

577 2. Barker MS, Arrigo N, Baniaga AE, Li Z, Levin DA. On the relative abundance of
578 autopolyploids and allopolyploids. New Phytol. 2015. doi:10.1111/nph.13698

579 3. Schoenfelder KP, Fox DT. The expanding implications of polyploidy. J Cell Biol.
580 2015;209: 485–491. doi:10.1083/jcb.201502016

581 4. Session AM, Uno Y, Kwon T, Chapman JA, Toyoda A, Takahashi S, et al. Genome
582 evolution in the allotetraploid frog Xenopus laevis. Nature. 2016;538: 336–343.
583 doi:10.1038/nature19840

584 5. Ming R, Man Wai C. Assembling allopolyploid genomes: no longer formidable.
585 Genome Biol. 2015;16: 27. doi:10.1186/s13059-015-0585-5

586 6. Kyriakidou M, Tai HH, Anglin NL, Ellis D, Strömvik MV. Current Strategies of
587 Polyploid Plant Genome Sequence Assembly. Front Plant Sci. 2018;9: 1660.
588 doi:10.3389/fpls.2018.01660

589 7. Rhie A, McCarthy SA, Fedrigo O, Damas J, Formenti G, Koren S, et al. Towards
590 complete and error-free genome assemblies of all vertebrate species. Nature. 2021;592:
591 737–746. doi:10.1038/s41586-021-03451-0

592 8. Zhang X, Wu R, Wang Y, Yu J, Tang H. Unzipping haplotypes in diploid and
593 polyploid genomes. Comput Struct Biotechnol J. 2020;18: 66–72.
594 doi:10.1016/j.csbj.2019.11.011
595 9. Saada OA, Friedrich A, Schacherer J. Towards accurate, contiguous and complete
596 alignment-based polyploid phasing algorithms. Genomics. 2022;114: 110369.
597 doi:10.1016/j.ygeno.2022.110369
598 10. Edger PP, Poorten TJ, VanBuren R, Hardigan MA, Colle M, McKain MR, et al. Origin
599 and evolution of the octoploid strawberry genome. Nat Genet. 2019;51: 541–547.
600 doi:10.1038/s41588-019-0356-4
601 11. Gan X, Li S, Zong Y, Cao D, Li Y, Liu R, et al. Chromosome-Level Genome
602 Assembly Provides New Insights into Genome Evolution and Tuberous Root
603 Formation of Potentilla anserina. Genes . 2021;12. doi:10.3390/genes12121993
604 12. Kolesnikova UK, Scott AD, Van de Velde JD, Burns R, Tikhomirov NP, Pfordt U, et
605 al. Genome of selfing Siberian Arabidopsis lyrata explains establishment of
606 allopolyploid Arabidopsis kamchatica. bioRxiv. 2022. p. 2022.06.24.497443.
607 doi:10.1101/2022.06.24.497443
608 13. Zheng Y, Yang D, Rong J, Chen L, Zhu Q, He T, et al. Allele-aware chromosome-
609 scale assembly of the allopolyploid genome of hexaploid Ma bamboo
610 (Dendrocalamus latiflorus Munro). J Integr Plant Biol. 2022;64: 649–670.
611 doi:10.1111/jipb.13217
612 14. Du K, Stöck M, Kneitz S, Klopp C, Woltering JM, Adolfi MC, et al. The sterlet
613 sturgeon genome sequence and the mechanisms of segmental rediploidization.
614 Nature Ecology & Evolution. 2020;4: 841–852. doi:10.1038/s41559-020-1166-x
615 15. Kuhl H, Du K, Schartl M, Kalous L, Stöck M, Lamatsch DK. Equilibrated evolution of
616 the mixed auto-/allopolyploid haplotype-resolved genome of the invasive hexaploid
617 Prussian carp. Nat Commun. 2022;13: 4092. doi:10.1038/s41467-022-31515-w

618 16. Perry RN, Moens M, Starr JL. Root-knot Nematodes. CABI; 2009. Available:
619 https://play.google.com/store/books/details?id=UN3uHMr_UCoC
620 17. Williamson VM, Gleason CA. Plant–nematode interactions. Curr Opin Plant Biol.
621 2003;6: 327–333. doi:10.1016/S1369-5266(03)00059-1
622 18. Trudgill DL, Blok VC. Apomictic, polyphagous root-knot nematodes: exceptionally
623 successful and damaging biotrophic root pathogens. Annu Rev Phytopathol.
624 2001;39: 53–77. doi:10.1146/annurev.phyto.39.1.53
625 19. Szitenberg A, Salazar-Jaramillo L, Blok VC, Laetsch DR, Joseph S, Williamson VM,
626 et al. Comparative Genomics of Apomictic Root-Knot Nematodes: Hybridization,
627 Ploidy, and Dynamic Genome Change. Genome Biol Evol. 2017;9: 2844–2861.
628 doi:10.1093/gbe/evx201
629 20. Wesemael W, Viaene N, Moens M. Root-knot nematodes (Meloidogyne spp.) in
630 Europe. Nematology. 2011;13: 3–16. doi:10.1163/138855410X526831
631 21. Jones JT, Haegeman A, Danchin EGJ, Gaur HS, Helder J, Jones MGK, et al. Top 10
632 plant-parasitic nematodes in molecular plant pathology. Mol Plant Pathol. 2013;14:
633 946–961. Available:
634 https://bsppjournals.onlinelibrary.wiley.com/doi/abs/10.1111/mpp.12057
635 22. Bernard GC, Egnin M, Bonsi C. The impact of plant-parasitic nematodes on
636 agriculture and methods of control. Nematology-Concepts, Diagnosis and Control.
637 2017;10. Available:
638 https://books.google.co.uk/bookshl=en&lr=&id=MQWQDwAAQBAJ&oi=fnd&pg=PA1
639 21&dq=agricultural+impact+root-knot+nematodes&ots=bBkbCxpflc&sig=1tg90hY-
640 8Y2Z7V_6F8KGljCENoM

641 23. Eisenback JD, Triantaphyllou HH. Root-knot nematodes: Meloidogyne species and
642 races. Manual of agricultural nematology. 1991;1: 191–274. Available:
643 https://www.researchgate.net/profile/Jonathan_Eisenback/publication/
644 283548298_Root-Knot_Nematodes_Meloidogyne_Species_and_Races/links/
645 563e67e308ae34e98c4d93c1/Root-Knot-Nematodes-Meloidogyne-Species-and-
646 Races.pdf
647 24. Subbotin SA, Rius JEP, Castillo P. Systematics of Root-knot Nematodes (Nematoda:
648 Meloidogynidae). BRILL; 2021. Available:
649 https://play.google.com/store/books/details?id=xs87EAAAQBAJ
650 25. Triantaphyllou AC. Gametogenesis and the Chromosomes of Meloidogyne nataliei:
651 Not Typical of Other Root-knot Nematodes. J Nematol. 1985;17: 1–5. Available:
652 https://www.ncbi.nlm.nih.gov/pubmed/19294050
653 26. Bird DM, Williamson VM, Abad P, McCarter J, Danchin EGJ, Castagnone-Sereno P,
654 et al. The genomes of root-knot nematodes. Annu Rev Phytopathol. 2009;47: 333–
655 351. doi:10.1146/annurev-phyto-080508-081839
656 27. Lunt DH. Genetic tests of ancient asexuality in root knot nematodes reveal recent
657 hybrid origins. BMC Evol Biol. 2008;8: 194. doi:10.1186/1471-2148-8-194
658 28. Blanc-Mathieu R, Perfus-Barbeoch L, Aury J-M, Da Rocha M, Gouzy J, Sallet E, et
659 al. Hybridization and polyploidy enable genomic plasticity without sex in the most
660 devastating plant-parasitic nematodes. PLoS Genet. 2017;13: e1006777.
661 doi:10.1371/journal.pgen.1006777
662 29. Hartman KM, Sasser JN. Identification of Meloidogyne species on the basis of
663 differential host test and perineal pattern morphology. An advanced treatise on
664 Meloidogyne. 1985;2: 69–77. Available: https://books.google.com/books?
665 hl=en&lr=&id=gNo4AQAAIAAJ&oi=fnd&pg=PA69&dq=hartman+and+sasser&ots=r0
666 T3kOF2TR&sig=qp5-qepxxIy-MaZ3Yxq8q3OTlBg

667 30. Roberts PA, Thomason J. Variability in reproduction of isolates of Meloidogyne
668 incognita and M. javanica on resistant tomato genotypes. worldveg.tind.io; 1986.
669 Available: https://worldveg.tind.io/record/4772/
670 31. Rammah A, Hirschmann H. Morphological Comparison of Three Host Races of
671 Meloidogyne javanica. J Nematol. 1990;22: 56–68. Available:
672 https://www.ncbi.nlm.nih.gov/pubmed/19287689
673 32. Williamson VM, Kumar A. Nematode resistance in plants: the battle underground.
674 Trends Genet. 2006;22: 396–403. doi:10.1016/j.tig.2006.05.003
675 33. Gleason CA, Liu QL, Williamson VM. Silencing a candidate nematode effector gene
676 corresponding to the tomato resistance gene Mi-1 leads to acquisition of virulence.
677 Mol Plant Microbe Interact. 2008;21: 576–585. doi:10.1094/MPMI-21-5-0576
678 34. Hajihassani A, Marquez J, Woldemeskel M, Hamidi N. Identification of Four
679 Populations of Meloidogyne incognita in Georgia, United States, Capable of
680 Parasitizing Tomato-Bearing Mi-1.2 Gene. Plant Dis. 2022;106: 137–143.
681 doi:10.1094/PDIS-05-21-0902-RE
682 35. Sato K, Kadota Y, Gan P, Bino T, Uehara T, Yamaguchi K, et al. High-Quality
683 Genome Sequence of the Root-Knot Nematode Meloidogyne arenaria Genotype A2-
684 O. Genome Announc. 2018;6. doi:10.1128/genomeA.00519-18
685 36. Susič N, Koutsovoulos GD, Riccio C, Danchin EGJ, Blaxter ML, Lunt DH, et al.
686 Genome sequence of the root-knot nematode Meloidogyne luci. J Nematol. 2020;52:
687 1–5. doi:10.21307/jofnem-2020-025
688 37. Fox DT, Soltis DE, Soltis PS, Ashman T-L, Van de Peer Y. Polyploidy: A biological
689 force from cells to ecosystems. Trends Cell Biol. 2020;30: 688–694.
690 doi:10.1016/j.tcb.2020.06.006

691 38. Ranallo-Benavidez TR, Jaron KS, Schatz MC. GenomeScope 2.0 and Smudgeplot
692 for reference-free profiling of polyploid genomes. Nat Commun. 2020;11: 1432.
693 doi:10.1038/s41467-020-14998-3
694 39. Cheng H, Concepcion GT, Feng X, Zhang H, Li H. Haplotype-resolved de novo
695 assembly using phased assembly graphs with hifiasm. Nat Methods. 2021;18: 170–
696 175. doi:10.1038/s41592-020-01056-5
697 40. Zimin AV, Salzberg SL. The SAMBA tool uses long reads to improve the contiguity of
698 genome assemblies. PLoS Comput Biol. 2022;18: e1009860.
699 doi:10.1371/journal.pcbi.1009860
700 41. Laetsch DR, Blaxter ML. BlobTools: Interrogation of genome assemblies. F1000Res.
701 2017;6: 1287. doi:10.12688/f1000research.12232.1
702 42. Parra G, Bradnam K, Korf I. CEGMA: a pipeline to accurately annotate core genes in
703 eukaryotic genomes. Bioinformatics. 2007;23: 1061–1067.
704 doi:10.1093/bioinformatics/btm071
705 43. Koutsovoulos GD, Poullet M, El Ashry A, Kozlowski DK, Sallet E, Da Rocha M, et al.
706 The polyploid genome of the mitotic parthenogenetic root-knot nematode
707 Meloidogyne enterolobii. bioRxiv. 2019. p. 586818. doi:10.1101/586818
708 44. Kozlowski DKL, Hassanaly-Goulamhoussen R, Da Rocha M, Koutsovoulos GD,
709 Bailly-Bechet M, Danchin EGJ. Movements of transposable elements contribute to
710 the genomic plasticity and species diversification in an asexually reproducing
711 nematode pest. Evol Appl. 2021;14: 1844–1866. doi:10.1111/eva.13246
712 45. Cerca J, Petersen B, Lazaro-Guevara JM, Rivera-Colón A, Birkeland S, Vizueta J, et
713 al. The genomic basis of the plant island syndrome in Darwin's giant daisies. Nat
714 Commun. 2022;13: 3729. doi:10.1038/s41467-022-31280-w

715 46. Koutsovoulos GD, Poullet M, Elashry A, Kozlowski DKL, Sallet E, Da Rocha M, et al.
716 Genome assembly and annotation of Meloidogyne enterolobii, an emerging
717 parthenogenetic root-knot nematode. Scientific Data. 2020;7: 324.
718 doi:10.1038/s41597-020-00666-0
719 47. Koutsovoulos GD, Marques E, Arguel M, Duret L, Machado ACZ, Carneiro RMDG,
720 et al. Population genomics supports clonal reproduction and multiple independent
721 gains and losses of parasitic abilities in the most devastating nematode pest. Evol
722 Appl. 2019;26: 909. doi:10.1111/eva.12881
723 48. Bali S, Hu S, Vining K, Brown C, Mojtahedi H, Zhang L, et al. Nematode genome
724 announcement: Draft genome of Meloidogyne chitwoodi, an economically important
725 pest of potato in the pacific northwest. Mol Plant Microbe Interact. 2021;
726 MPMI12200337A. doi:10.1094/MPMI-12-20-0337-A
727 49. Mason JM, Reddy HM, Frydrychova RC. Telomere Maintenance in Organisms
728 without Telomerase. In: Seligmann H, editor. DNA Replication. Rijeka: IntechOpen;
729 2011. doi:10.5772/19348
730 50. Pardue M-L, DeBaryshe PG. Retrotransposons that maintain chromosome ends.
731 Proc Natl Acad Sci U S A. 2011;108: 20317–20324. doi:10.1073/pnas.1100278108
732 51. Jaron KS, Bast J, Nowell RW, Ranallo-Benavidez TR, Robinson-Rechavi M,
733 Schwander T. Genomic Features of Parthenogenetic Animals. J Hered. 2021;112:
734 19–33. doi:10.1093/jhered/esaa031
735 52. Edger PP, McKain MR, Bird KA, VanBuren R. Subgenome assignment in
736 allopolyploids: challenges and future directions. Curr Opin Plant Biol. 2018;42: 76–
737 80. doi:10.1016/j.pbi.2018.03.006

738 53. Emery M, Willis MMS, Hao Y, Barry K, Oakgrove K, Peng Y, et al. Preferential
739 retention of genes from one parental genome after polyploidy illustrates the nature
740 and scope of the genomic conflicts induced by hybridization. PLoS Genet. 2018;14:
741 e1007267. doi:10.1371/journal.pgen.1007267
742 54. Ma X-F, Gustafson JP. Genome evolution of allopolyploids: a process of cytological
743 and genetic diploidization. Cytogenet Genome Res. 2005;109: 236–249.
744 doi:10.1159/000082406
745 55. Balloux F, Lehmann L, de Meeûs T. The Population Genetics of Clonal and Partially
746 Clonal Diploids. Genetics. 2003;164: 1635–1644. doi:10.1093/genetics/164.4.1635
747 56. Carlton PM, Davis RE, Ahmed S. Nematode chromosomes. Genetics. 2022.
748 doi:10.1093/genetics/iyac014
749 57. Masterson J. Stomatal size in fossil plants: evidence for polyploidy in majority of
750 angiosperms. Science. 1994;264: 421–424. doi:10.1126/science.264.5157.421
751 58. Shen Y, Li W, Zeng Y, Li Z, Chen Y, Zhang J, et al. Chromosome-level and
752 haplotype-resolved genome provides insight into the tetraploid hybrid origin of
753 patchouli. Nat Commun. 2022;13: 1–15. doi:10.1038/s41467-022-31121-w
754 59. Dodsworth S, Chase MW, Leitch AR. Is post-polyploidization diploidization the key to
755 the evolutionary success of angiosperms? Bot J Linn Soc. 2016;180: 1–5.
756 doi:10.1111/boj.12357
757 60. Harris S, Rudnicki KS, Haber JE. Gene conversions and crossing over during
758 homologous and homeologous ectopic recombination in Saccharomyces cerevisiae.
759 Genetics. 1993;135: 5–16. doi:10.1093/genetics/135.1.5
760 61. Mansai SP, Innan H. The power of the methods for detecting interlocus gene
761 conversion. Genetics. 2010;184: 517–527. doi:10.1534/genetics.109.111161
762 62. Hollister JD. Polyploidy: adaptation to the genomic environment. New Phytol.
763 2015;205: 1034–1039. doi:10.1111/nph.12939

764 63. Paquin C, Adams J. Frequency of fixation of adaptive mutations is higher in evolving
765 diploid than haploid yeast populations. Nature. 1983;302: 495–500.
766 doi:10.1038/302495a0
767 64. Otto SP, Whitton J. Polyploid incidence and evolution. Annu Rev Genet. 2000;34:
768 401–437. doi:10.1146/annurev.genet.34.1.401
769 65. Zörgö E, Chwialkowska K, Gjuvsland AB, Garré E, Sunnerhagen P, Liti G, et al.
770 Ancient evolutionary trade-offs between yeast ploidy states. PLoS Genet. 2013;9:
771 e1003388. doi:10.1371/journal.pgen.1003388
772 66. Castagnone-Sereno P, Mulet K, Danchin EGJ, Koutsovoulos GD, Karaulic M, Da
773 Rocha M, et al. Gene copy number variations as signatures of adaptive evolution in
774 the parthenogenetic, plant-parasitic nematode Meloidogyne incognita. Mol Ecol.
775 2019;26: 906. doi:10.1111/mec.15095
776 67. Pogorelko GV, Juvale PS, Rutter WB, Hütten M, Maier TR, Hewezi T, et al. Re-
777 targeting of a plant defense protease by a cyst nematode effector. Plant J. 2019;98:
778 1000–1014. doi:10.1111/tpj.14295
779 68. Kihika R, Tchouassi DP, Ng'ang'a MM, Hall DR, Beck JJ, Torto B. Compounds
780 Associated with Infection by the Root-Knot Nematode, Meloidogyne javanica,
781 Influence the Ability of Infective Juveniles to Recognize Host Plants. J Agric Food
782 Chem. 2020;68: 9100–9109. doi:10.1021/acs.jafc.0c03386
783 69. Song H, Lin B, Huang Q, Sun T, Wang W, Liao J, et al. The Meloidogyne javanica
784 effector Mj2G02 interferes with jasmonic acid signalling to suppress cell death and
785 promote parasitism in Arabidopsis. Mol Plant Pathol. 2021;22: 1288–1301.
786 doi:10.1111/mpp.13111
787 70. Sellers GS, Jeffares DC, Lawson B, Prior T, Lunt DH. Identification of individual root-
788 knot nematodes using low coverage long-read sequencing. PLoS One. 2021;16:
789 e0253248. doi:10.1371/journal.pone.0253248

790 71. PacificBiosciences. IsoSeq3. Github; 2022. Available:
791 https://github.com/PacificBiosciences/IsoSeq
792 72. Winter M. asmapp: ASMAPP assembly appraisal workflow. Built in snakemake,
793 ASMAPP performs many basic and intermediate assembly appraisal tasks. Github;
794 2022. Available: https://github.com/mrmrwinter/asmapp
795 73. Guan D, McCarthy SA, Wood J, Howe K, Wang Y, Durbin R. Identifying and
796 removing haplotypic duplication in primary genome assemblies. Bioinformatics.
797 2020;36: 2896–2898. doi:10.1093/bioinformatics/btaa025
798 74. Luo J, Lyu M, Chen R, Zhang X, Luo H, Yan C. SLR: a scaffolding algorithm based
799 on long reads and contig classification. BMC Bioinformatics. 2019;20: 1–11.
800 doi:10.1186/s12859-019-3114-9
801 75. Durand NC, Robinson JT, Shamim MS, Machol I, Mesirov JP, Lander ES, et al.
802 Juicebox Provides a Visualization System for Hi-C Contact Maps with Unlimited
803 Zoom. Cell Syst. 2016;3: 99–101. doi:10.1016/j.cels.2015.07.012
804 76. Smit AFA, Hubley R, Green P. RepeatModeler Open-1.0. 2008--2015. Seattle, USA:
805 Institute for Systems Biology Available from: httpwww repeatmasker org, Last
806 Accessed May. 2015;1: 2018.
807 77. Smit AFA, Hubley R, Green P. RepeatMasker Open-4.0. 2013--2015. 2015.
808 78. Holt C, Yandell M. MAKER2: an annotation pipeline and genome-database
809 management tool for second-generation genome projects. BMC Bioinformatics.
810 2011;12: 491. doi:10.1186/1471-2105-12-491
811 79. Campbell MS, Holt C, Moore B, Yandell M. Genome Annotation and Curation Using
812 MAKER and MAKER-P. Curr Protoc Bioinformatics. 2014;48: 4.11.1–39.
813 doi:10.1002/0471250953.bi0411s48

814 80. Ondov BD, Treangen TJ, Melsted P, Mallonee AB, Bergman NH, Koren S, et al.
815 Mash: fast genome and metagenome distance estimation using MinHash. Genome
816 Biol. 2016;17: 132. doi:10.1186/s13059-016-0997-x
817 81. Simão FA, Waterhouse RM, Ioannidis P, Kriventseva EV, Zdobnov EM. BUSCO:
818 assessing genome assembly and annotation completeness with single-copy
819 orthologs. Bioinformatics. 2015;31: 3210–3212. doi:10.1093/bioinformatics/btv351
820 82. Marçais G, Kingsford C. A fast, lock-free approach for efficient parallel counting of
821 occurrences of k-mers. Bioinformatics. 2011;27: 764–770.
822 doi:10.1093/bioinformatics/btr011
823 83. Tang H, Bowers JE, Wang X, Ming R, Alam M, Paterson AH. Synteny and
824 collinearity in plant genomes. Science. 2008;320: 486–488.
825 doi:10.1126/science.1153917
826 84. Tang H, Krishnakumar V, Li J. jcvi: JCVI utility libraries. 2015.
827 doi:10.5281/zenodo.31631
828 85. Altschul SF, Gish W, Miller W, Myers EW, Lipman DJ. Basic local alignment search
829 tool. J Mol Biol. 1990;215: 403–410. doi:10.1016/S0022-2836(05)80360-2
830 86. Bernt M, Donath A, Jühling F, Externbrink F, Florentz C, Fritzsch G, et al. MITOS:
831 improved de novo metazoan mitochondrial genome annotation. Mol Phylogenet
832 Evol. 2013;69: 313–319. doi:10.1016/j.ympev.2012.08.023
833 87. Li H, Handsaker B, Wysoker A, Fennell T, Ruan J, Homer N, et al. The Sequence
834 Alignment/Map format and SAMtools. Bioinformatics. 2009;25: 2078–2079.
835 doi:10.1093/bioinformatics/btp352
836 88. Gurevich A, Saveliev V, Vyahhi N, Tesler G. QUAST: quality assessment tool for
837 genome assemblies. Bioinformatics. 2013;29: 1072–1075.
838 doi:10.1093/bioinformatics/btt086
839

840

841 # Supporting information

842 **S1 Fig: Length and quality statistics of concatenated and quality controlled PacBio**
843 **HiFi libraries.**

844 **S2 Fig: Length and quality statistics of concatenated and quality controlled Oxford**

845 **Nanopore libraries.**

846 **S3 Fig: Total cumulative length over number of scaffolds.**

847 **S4 Fig: Blobplot of contamination in our *Meloidogyne javanica* assembly**

848 **S5 Fig: BUSCO v5 results.**

849 **S6 Fig: Assembly-wide distributions of coverage**

850 **S7 Fig: Scaffold-level distributions of coverage**

851 **S8 Fig: Coverage depth of individual bases across scaffolds.**

852 **S9 Fig: Subgenome phased dendrogram of scaffolds.**

853 **S1 Table: Descriptive statistics of assembly and its contemporaries**

854 **S2 Table: Tabular breakdown of repeat annotation from *RepeatMasker*.**

855 **S3 Table: Full table of results from structural annotation with MAKER3.**

856 **S4 Table: List of pairs that share CDS and amount of shared links.**

857 **S5 Table: Validation of homoeologous pairings.**

858 **S6 Table: Summary of the longest 33 scaffolds.**